CHEMBIOCHEM

DOI: 10.1002/cbic.200900008

Thermodynamic and Computational Studies on the Binding of p53-Derived Peptides and Peptidomimetic Inhibitors to HDM2

Anja Grässlin, Celine Amoreira, Kim K. Baldridge,* and John A. Robinson*[a]

The human double minute 2 protein (HDM2) binds a short peptide derived from the N terminus of the tumor-suppressor protein, p53. This peptide (p53 residues 15–29) is flexible in free solution, but upon binding to HDM2 it folds into an amphipathic α-helical conformation. Three residues along one face of the p53 helix (Phe19, Trp23, and Leu26) dock into hydrophobic pockets on the surface of HDM2. A conformationally constrained cyclic β-hairpin peptidomimetic of p53, with residues Phe1, 6-chloro-Trp3, and Leu4 in one strand of the β-hairpin, was shown earlier to dock into the same pockets on HDM2. Here, we show by isothermal titration calorimetry that the entropy loss upon binding of the constrained peptide to HDM2 is, as would be expected, much lower ($T\Delta S \approx 10$ kcal mol^{-1} at 300 K) than that for the linear peptide. However, the entropic advantage enjoyed by the constrained peptide is largely offset by a reduced enthalpic contribution, relative to the linear peptide, to binding of the cyclic mimetic. To explore the electronic nature of the interactions between the energetically important residues in each ligand and HDM2, hybrid quantum mechanical and electrostatic Poisson–Boltzmann computational studies were performed. The calculations reveal that significant stabilizing van der Waals interactions and polarization effects occur between the Trp side chain in each ligand and aromatic and aliphatic residues in HDM2. These stabilizing interactions are enhanced when a 6-chloro substituent is incorporated into the Trp, in agreement with the experimental studies. In addition, the calculations suggest that at least one stabilizing hydrogen bond is formed, between the Trp indole-NH in both ligands and HDM2. Other hydrogen-bonding interactions also arise, however, along the α-helical backbone of the linear peptide upon binding to HDM2, but are not mimicked in the constrained inhibitor–HDM2 complex. The formation of these hydrogen bonds upon helix folding could contribute significantly to the enhanced enthalpy observed in binding of the linear peptide to HDM2.

Introduction

The interaction of p53 with the human equivalent of the mouse double minute 2 protein (HDM2) has become an interesting model system for the design of new protein–protein interaction inhibitors.[1] Such studies have been spurred on by the important antitumor activity of the transcription factor p53, which functions to prevent the emergence and propagation of cancer-prone cells.[2] Inhibitors of the p53–HDM2 interaction have also attracted pharmaceutical interest for their potential value in cancer therapy.[3,4]

HDM2 binds a short N-terminal segment of p53 (residues 15–29) in an amphipathic α-helical conformation with a dissociation constant (K_D) of about 600 nM.[5] An X-ray structure (PDB ID: 1YCR) reveals side chains of three residues (Phe19, Trp23, and Leu26) aligned along one face of the p53 helix, and these dock into hydrophobic pockets on the surface of HDM2 (Figure 1). Two hydrogen bonds between the ligand and the protein are also identified: one between the Phe19 backbone amide NH of p53 and the carbonyl group of the Gln72 side chain in HDM2, and another between the p53 Trp23 indole NH and the HDM2 Leu54 backbone carbonyl.

A large number of peptidic and small-molecule p53/HDM2 inhibitors that target the p53-binding pockets on HDM2 have been described in recent years (reviewed in refs. [1] and [4]). One example is the linear phage-derived peptide **1**, which inhibits the p53–HDM2 interaction with an IC_{50} value of 8.9 μM, as determined by competition ELISA.[6] Improvement of this lead compound gave peptide **2**, with an IC_{50} value of 314 nM. A further significant increase in affinity was achieved by incorporation of a halogen at the 6-position of the tryptophan indole moiety. This discovery was prompted by a careful analysis of the p53·HDM2 crystal structure,[5] which revealed a small cavity at the bottom of the Trp binding pocket that might be filled by a substituent the size of a methyl group or a chlorine atom at the indole 6-position. Indeed, peptides containing 6-chloro-, 6-methyl-, and 6-fluorotryptophan (6Cl-Trp, 6Me-Trp, 6F-Trp; **3**–**5**) had significantly improved binding affinities (IC_{50} = 5 nM (**3**), 10 nM (**4**), and 14 nM (**5**)).[6] Recently, a crystal

[a] *Dr. A. Grässlin, Dr. C. Amoreira, Prof. K. K. Baldridge,[+] Prof. J. A. Robinson[+]*
Department of Chemistry, Institute of Organic Chemistry
University of Zürich, Winterthurerstrasse 190
8057 Zürich (Switzerland)
Fax: (+41) 44-635-6833
E-mail: kimb@oci.uzh.ch
robinson@oci.uzh.ch

[+] *Please address queries concerning experimental methods to J.A.R. and queries concerning computations to K.K.B.*

Supporting information for this article is available on the WWW under http://dx.doi.org/10.1002/cbic.200900008; experimental details and computational methods.

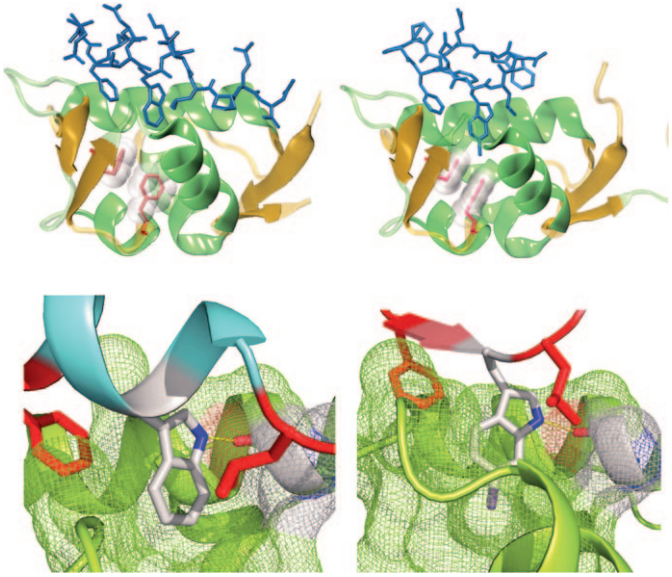

Figure 1. Top panels: the p53-derived peptide **13a**·HDM2 complex (PDB ID: 1YCR, left), and the β-hairpin peptidomimetic **7**·HDM2 complex (PDB ID: 2AXI, right). The conformations of the Phe86 and Phe91 side chains (in pink with CPK surface) are also shown. Lower panels: close-up views of the H-bond interactions involving the Trp indole NH in 1YCR (left) and 2AXI (right).

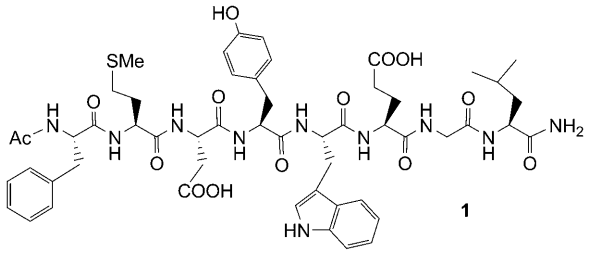

1

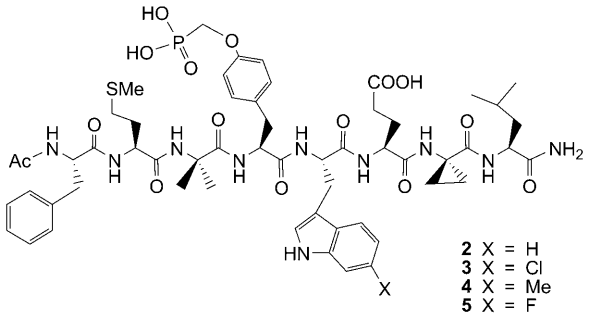

2 X = H
3 X = Cl
4 X = Me
5 X = F

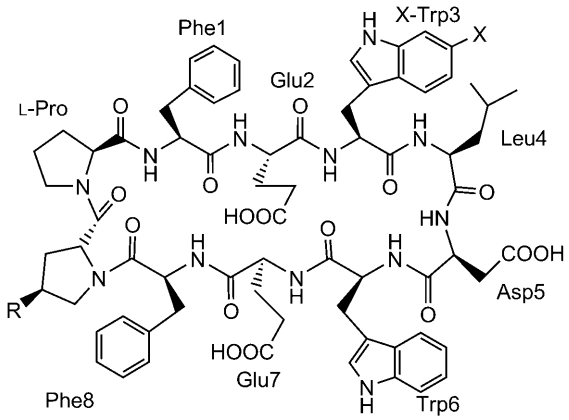

Cyclic peptidomimetics	X	R
6	H	H
7	Cl	H
8	Me	H
9	H	NHNH-Ac
10	H	NHNH-PEG-biotin
11	Cl	NHNH-PEG-biotin
12	Me	NHNH-PEG-biotin

NHNH-PEG-biotin =

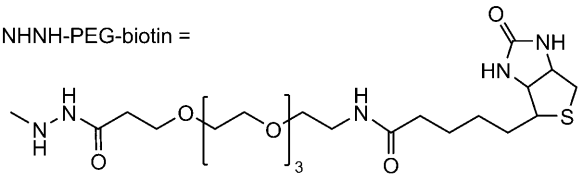

Linear peptides

13 Ac-SQETFSDLWKLLPEN-NH_2
13a SQETFSDLWKLLPEN
14 Ac-SQETFSDL-(6Cl)W-KLLPEN-NH_2
15 Ac-SQETFSDL-(6Me)W-KLLPEN-NH_2
16 Biotin-SGSGSQETFSDLWKLLPEN-NH_2
17 Biotin-SGSGSQETFSDL-(6Cl)W-KLLPEN-NH_2
18 Biotin-SGSGSQETFSDL-(6Me)W-KLLPEN-NH_2
19 Ac-FEWLDWEF-NH_2

Scheme 1. Structures of cyclic β-hairpin peptidomimetics (**6**–**12**) and linear p53-derived peptides (**13**–**19**) used in this work. The standard single-letter amino acid code is used for the linear peptides, except for the 6-substituted tryptophans (6Cl- or 6Me-W).

structure of peptide **3** bound to HDM2 confirmed that the Cl substituent indeed binds in and fills the Trp23 binding pocket.[7] Indeed, it is notable that chloro- and bromoaromatic groups in many small-molecule HDM2 inhibitors, including various *cis*-imidazolines[4] (also called Nutlins) and benzodiazepinediones,[8] bind with their halogen atoms located in the Trp23 binding pocket on HDM2.

We have previously reported cyclic β-hairpin peptidomimetics that mimic the α-helical epitope in p53 and bind to HDM2.[9,10] The optimized mimetic **7** contains Phe1, 6Cl-Trp3 and Leu4, along one strand of the hairpin (Scheme 1). A crystal structure of cyclic peptide **7** bound to HDM2 confirmed the β-hairpin backbone conformation of the inhibitor with the Phe1, 6Cl-Trp3 and Leu4 side chains occupying the expected p53 binding pockets (for Phe19, Trp23, and Leu26) on HDM2 (Figure 1).[9]

In this work, we set out to compare the thermodynamic signatures and the electronic natures of the stabilizing interactions occurring between p53-derived linear peptides (**13**–**15**) or cyclic β-hairpin inhibitors (**6**–**8**) and the p53 binding pockets on HDM2, using both experimental and theoretical methods.

Results

Experimental studies

The affinities of cyclic peptidomimetics and linear p53-derived peptides (residues 15–29) towards recombinant HDM2 (rHDM2) were measured in three ways. Firstly, a previously reported competitive surface plasmon resonance (SPR) binding assay,[10] was used to determine IC_{50} values. This assay involves immobilization of a biotinylated p53-derived linear peptide (**16**, Scheme 1) on a streptavidin-coated SPR biosensor surface, with rHDM2 and various concentrations of the inhibitor in the flow buffer. The IC_{50} is the concentration of inhibitor in the flow buffer required to reduce rHDM2 binding to the surface (SPR signal) by 50%. Secondly, dissociation constants (K_D values) were measured by SPR with biotinylated linear or cyclic peptides (**10**–**12** and **16**–**18**) immobilized on streptavidin-coated biosensor surfaces, with various concentrations of rHDM2 in the flow buffer. It was not possible to immobilize the rHDM2 directly on the biosensor surface without loss of biological activity. For biotinylation of the cyclic mimetics, a 4-hydrazino group was introduced into the pyrrolidine ring of the D-Pro residue (see the Supporting Information), and biotin was coupled to this through a short poly(ethylene glycol) linker (Scheme 1). The crystal structure of the **7**·HDM2 complex[9] showed that the 4-position in D-Pro is solvent-exposed and that a new substituent here is unlikely to influence HDM2 binding. Thirdly, K_D values for unmodified ligands (**6**–**8** and **13**–**15**) were determined by isothermal titration calorimetry (ITC) in free solution.

The IC_{50} value measured for cyclic peptide **9** (0.53 ± 0.05 μM) was essentially the same as that found for **6** (0.53 ± 0.06 μM), showing that (as would be expected) the acetylated hydrazino group does not significantly alter the interaction of the mimetic with rHDM2. The K_D values for binding of the biotinylated cyclic peptides **10**–**12** and the biotinylated linear peptides **16**–**18** to rHDM2, measured by SPR, are shown in Table 1. In addition, the affinity of the linear peptide **19**, which corresponds to the loop of cyclic peptide **7** without the D-Pro-L-Pro template, was measured. An IC_{50} value of 35 μM was determined by the competition assay, but the affinity was too weak to be determined by ITC. We conclude, therefore, that the constrained conformation of the macrocyclic peptide (**7**), and not just the loop sequence, is important for recognition by HDM2.

Table 1. Dissociation constants (K_D) determined by SPR for the interactions of **10**–**12** and **16**–**18** with rHDM2 at 298 K. Measurements were performed in triplicate and the means and deviations are shown.

Ligand (substituent)	K_D [μM]	Normalized $1/K_D$ [ΔG kcal mol^{-1}]
10 (X = H)	0.12 ± 0.01	1
11 (X = Cl)	0.065 ± 0.02	1.85 (0.36)
12 (X = Me)	0.27 ± 0.07	0.43 (−0.50)
16	0.67 ± 0.07	1
17 (+Cl)	0.055 ± 0.005	12.2 (1.48)
18 (+Me)	0.11 ± 0.01	6.1 (1.07)

The interactions of the unmodified linear peptides **13**–**15** and the cyclic peptides **6**–**8** with rHDM2 were next studied by ITC. Typical isotherms are shown in Figure 2, and the resulting thermodynamic parameters are given in Table 2 and are summarized in Figure 3 A.

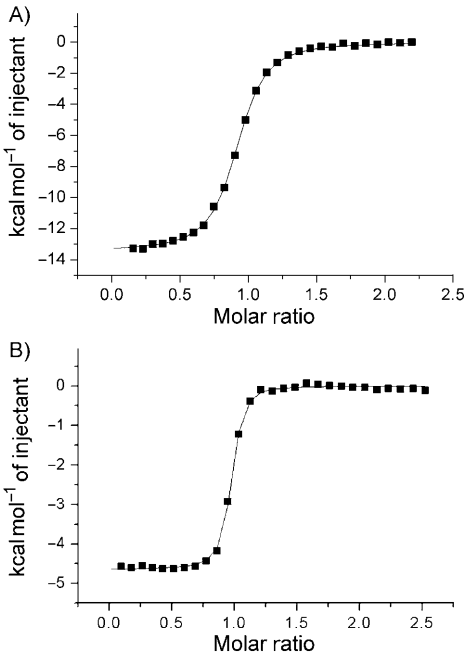

Figure 2. ITC isotherms for the binding of: A) linear peptide **13**, and B) cyclic peptidomimetic **7** to rHDM2.

Finally, the effects of substituting each residue in the cyclic peptide **7** (except the template residues D-Pro-L-Pro) by alanine (an alanine scan) on the binding affinities to rHDM2 were determined. The results (Table 3) show that the most pronounced losses in affinity (>300-fold) are seen upon substitution either of 6Cl-Trp3 or Phe1, whereas substitutions of Leu4, Asp5, or Trp6 each caused approximately tenfold losses in affinity. The Glu2Ala and Glu7Ala mutants also show reduced affinities, although these side chains are solvent-exposed, do not make contacts with HDM2, and so would not be expected to contribute significantly to binding.[9] In these two cases, however, the solubilities of the peptides in water are dramatically reduced, and both peptides aggregate even at low concentrations in aqueous solution, as evidenced by extremely broad ^{1}H NMR signals in spectra measured in aqueous solution (data not shown). In addition, the ITC data for these two mutants showed biphasic isotherms, which were not consistent with a simple 1:1 binding model, although inhibitory activity could be detected by SPR (not shown). The altered binding affinities for these two mutants, therefore, reflect complex processes arising from a major change in the physical properties of the peptides, affecting solubility and aggregation.

Table 2. Ligand binding to rHDM2 measured by isothermal titration calorimetry at 298 K. Measurements were performed at least in duplicate and the means and deviations are shown.

Ligand (substituent)	ΔH° [kcal mol^{-1}]	$T\Delta S$ [kcal mol^{-1}]	Stoichiometry	K_D [μM]	Normalized $1/K_D$ [ΔG kcal mol^{-1}]
6 (H)	−4.6 ± 0.1	+5.1 ± 0.2	0.94 ± 0.03	0.073 ± 0.005	1.0
7 (Cl)	−4.6 ± 0.1	+5.8 ± 0.4	0.92 ± 0.02	0.025 ± 0.002	2.92 (0.63)
8 (Me)	−3.9 ± 0.1	+5.7 ± 0.2	0.94 ± 0.1	0.10 ± 0.02	0.73 (−0.19)
13 (H)	−14.1 ± 0.7	−5.4 ± 0.7	0.91 ± 0.1	0.43 ± 0.03	1.0
14 (Cl)	−15.8 ± 0.6	−6.1 ± 0.5	1.01 ± 0.1	0.08 ± 0.01	5.38 (1.00)
15 (Me)	−14.7 ± 0.6	−5.1 ± 0.7	1.00 ± 0.09	0.09 ± 0.06	4.78 (0.93)

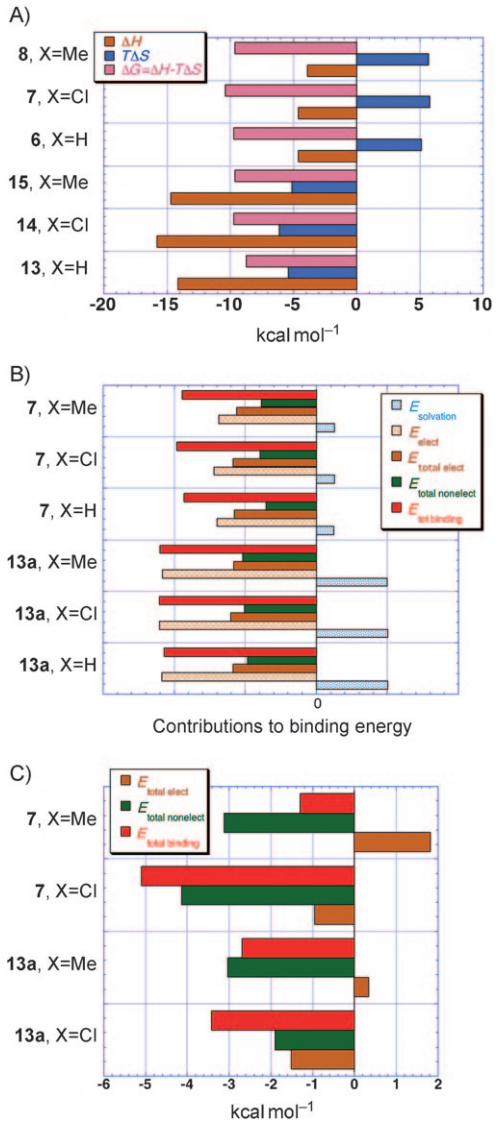

Figure 3. A) Comparison of the experimentally measured thermodynamic signatures of binding to rHDM2 for the linear (**13**–**15**) and cyclic (**6**–**8**) peptides. B) Comparison of the calculated binding energies determined by the APBS method (see text) for the linear and cyclic peptides. C) Theoretical electrostatic binding energy differences determined for the ligands with X = Cl or X = Me, relative to the corresponding peptide containing tryptophan (X = H).

Computational studies

As an aid in the characterization of the electronic nature of the interactions between HDM2 and the three linear p53-derived peptides (**13**–**15**) and the three cyclic β-hairpin peptidomimetics (**6**–**8**), we have used several strategies involving computational quantum chemistry and hybrid quantum/classical electrostatic methods (see the Supporting Information, computational methods).

Firstly, unconstrained density functional theory optimizations were performed on each ligand, to provide accurate structure and electronic property data. These data were also used for subsequent hybrid-classical electrostatic studies. Unconstrained geometry searches were also performed on ligand plus selected surrounding HDM2 residue fragments, for better understanding of the electronic natures of these interactions.

Starting from the structure of the HDM2·**7** complex (PDB ID: 2AXI) assessment of van der Waals interactions between the ligand containing the 6-X-Trp component (where X = H, Cl or Me) and the HDM2 residues Phe86/Phe91 was carried out. Assessments were made for both the crystal structure conformation, and after an unconstrained geometry optimization, of each complex. Computations were performed both in vacuum and in a low-dielectric environment to mimic the protein. The results are shown in Table 4.

The indole NH of the 6-X-Trp residue in each of the three ligands **3**, **7**, and **13a** bound to HDM2 (PDB ID: 2V2, 2AXI, and 1YCR) is close enough (2.7 Å for O···N in 2AXI) to hydrogen bond to the backbone carbonyl group of Leu54 in HDM2 (Figure 1). We therefore used the X-ray structure of the **7**·HDM2 complex (2AXI) and computational methods to estimate the strength of this ligand–protein H-bond, how it changes when the 6-X-Trp substituent is varied, and thus whether it is likely to contribute to the stabilization of the ligand–HDM2 complex. The results of these calculations are shown in Table 5.

Next, hybrid quantum/classical electrostatic methods were used to investigate the entire ligand–HDM2 complex computationally, for each of the modified ligands considered. These computations incorporate the accurate QM structural and atomic charge data for the peptides. The calculated total binding energy ($\Delta E_{\text{tot binding}}$) was calculated by the Adaptive Poisson–Boltzmann Solver (APBS) method,[11] which includes electrostatic interactions ($\Delta E_{\text{tot elect}}$) arising from both Coulombic (ΔE_{elect}) and polar solvation ($\Delta E_{\text{solvation}}$) contributions, as well as nonpolar solvation effects ($\Delta E_{\text{tot nonelect}}$) arising from cavitation and dispersion terms; that is [Eqs (1), (2), (3)]:

$$\Delta E_{\text{tot binding}} = \Delta E_{\text{tot elect}} + \Delta E_{\text{tot nonelect}} \quad (1)$$

where:

$$\Delta E_{\text{tot elect}} = \Delta E_{\text{elect}} + \Delta E_{\text{solvation}} \quad (2)$$

Table 3. The effects of an alanine scan with inhibitor **7** (residues 1 to 8 are shown). The D-Pro-L-Pro template was not altered. Mean values for ΔH, $T\Delta S$, and K_d are derived from at least two independent ITC experiments. Mean inhibitory activities (IC_{50}) and standard deviations are derived from at least three independent SPR-based inhibition assay experiments.

Peptide	Residue								ΔH	$T\Delta S$	K_d [μM]	IC_{50} [μM]
	1	2	3	4	5	6	7	8	[kcal mol^{-1}]	[kcal mol^{-1}]	(ITC)	(SPR)
7	F	E	$^{(6Cl)}$W	L	D	W	E	F	-4.6 ± 0.1	$+5.8\pm0.2$	0.025 ± 0.002	0.14 ± 0.06
20	A	E	$^{(6Cl)}$W	L	D	W	E	F	-4.8 ± 0.2	$+2.1\pm0.2$	9.0 ± 0.4	7 ± 3
21	F	A	$^{(6Cl)}$W	L	D	W	E	F	–[a]	–[a]	–[a]	1.1 ± 0.4
22	F	E	A	L	D	W	E	F	–[a]	–[a]	–[a]	23 ± 8
23	F	E	$^{(6Cl)}$W	A	D	W	E	F	-6.1 ± 0.4	$+2.7\pm0.4$	0.35 ± 0.04	0.55 ± 0.07
24	F	E	$^{(6Cl)}$W	L	A	W	E	F	-2.2 ± 0.1	$+6.7\pm0.03$	0.28 ± 0.03	0.35 ± 0.05
25	F	E	$^{(6Cl)}$W	L	D	A	E	F	-7.3 ± 0.1	$+1.5\pm0.1$	0.36 ± 0.01	0.70 ± 0.01
26	F	E	$^{(6Cl)}$W	L	D	W	A	F	–[a]	–[a]	–[a]	0.60 ± 0.1
27	F	E	$^{(6Cl)}$W	L	D	W	E	A	-8.4 ± 0.2	$+1.2\pm0.2$	0.095 ± 0.003	0.18 ± 0.02

[a] "–" indicates an interaction either too weak to analyze or, in the case of peptides **21** and **26**, showing biphasic behavior.

Table 4. Calculated interaction energies [kcal mol^{-1}] between Phe86/Phe91 of HDM2 and X-Trp in the cyclic peptidomimetics (**6**–**8**) in the crystal structure PDB 2AXI.

Trp-X	E [kcal mol^{-1}]		Shortest X to Phe hydrogen distances [Å][a]	
	gas phase	$\varepsilon=4$	X–Phe86-H	X–Phe91-H
X = H	0.7	0.0	2.7, 2.8	2.2, 2.4
X = Cl	2.4	1.5	3.3, 3.1	2.9, 2.8
X = Me	1.2	0.7	2.7, 3.0	2.3, 2.4

[a] X–Phe86 distance of the two closest Phe hydrogens; X–Phe91 distance of the two closest Phe hydrogens; the shortest distances found in the crystal structure are 3.4 Å and 3.6–3.7 Å, respectively.

Table 5. Assessment of H-bond energies [kcal mol^{-1}] and distances between Leu54 of HDM2 and X-Trp in the cyclic peptidomimetics **6**–**8**.

System	H-bond energy, dipole moment, and N···H···O distances[a]				
2AXI + X-Trp	E [kcal mol^{-1}]		Dipole	H-bond distances	
	$\varepsilon=1$	$\varepsilon=4$	(D)	N–O	N–H/H···O
X = H	4.5	2.1	3.8	2.96	1.02/2.00
X = Cl	5.2	2.5	5.0	2.92	1.01/2.06
X = Me	4.6	2.3	4.9	2.88	1.01/2.06

[a] M06-2X/DZ(2d,p) theory was used; calculated with the crystal structure (2AXI) and with the substituents X = H and X = CH_3 hydrogen bond optimized.

Each of these energies is evaluated for the complex (E) and for the separated protein ($E_{protein}$) and the ligand (E_{ligand}); that is:

$$\Delta E = E_{complex} - (E_{protein} + E_{ligand}) \quad (3)$$

The results of these calculations are represented in schematic form in Figure 3.

Discussion

Background information

The binding of HDM2 to helical and hairpin peptide ligands represents an interesting model system with which to explore the molecular basis of specific, high-affinity protein–ligand and protein–protein interactions. Although such interactions are key to many biological processes, it is still extraordinarily difficult to use high-resolution structural information on proteins and the complexes that they form either to predict binding affinities or to design de novo new molecules able to bind selectively and with high affinity to a chosen target.

In previous work, we showed how cyclic β-hairpin peptidomimetics such as **7** could be designed to mimic the helical epitope in p53 and to bind with high affinity to HDM2. Four crystal structures of peptide ligands bound to HDM2 are currently available: 1) with bound linear p53-derived peptide **13a** (PDB ID: 1YCR, resolution 2.6 Å),[5] 2) with bound phage-derived linear peptides, including **3** (PDB ID: 1T4F and 2V2, resolution 1.8 Å),[7,8] and 3) with bound cyclic peptide **7** (PDB ID: 2AXI, resolution 1.4 Å).[9] These structures reveal that residues along one face of the helix in **13a** (Phe19, Trp23, and Leu26) and the analogue **3** (Phe1, 6-chloro-Trp5, and Leu8) dock into three hydrophobic pockets on the surface of HDM2. In addition, residues Phe1, 6-chloro-Trp3, and Leu4 in one strand of the β-hairpin mimetic **7** dock similarly into the corresponding pockets on HDM2. The relative positions both of the HDM2 residues and of the Phe/(Cl)Trp/Leu triad in each ligand are very similar (with some qualification; see below) in the three structures 1YCR + 2V2 + 2AXI (Figure 4).

NMR spectroscopy studies have also provided important insights into the complex dynamic behavior of the p53–HDM2 system. Firstly, the N-terminal region of p53 (approximately residues 1–100 of the 393 amino acid protein), which includes the transactivation domain and a proline-rich region, is devoid of tertiary structure and largely lacks secondary structure elements in aqueous solution.[12,13] N-terminal p53-derived peptides adopt at best loosely folded, or nascent, helices and only become fully helical upon binding to HDM2.[14] Secondly, ligand-free HDM2 also appears by NMR spectroscopy to undergo significant conformational changes upon binding to p53, and to be considerably more flexible than the ligand-bound form.[15,16] Moreover, the p53-binding cleft in ligand-free HDM2 is mostly occluded as a result of the inward movement of two helices comprising the walls of the p53 binding cleft.[16] Before

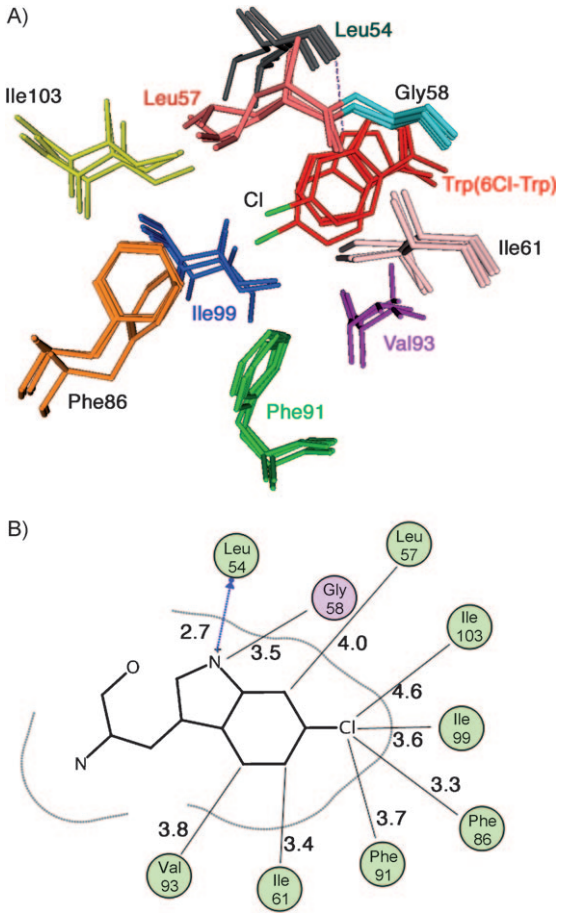

Figure 4. A) Backbone superimposition of the p53-binding pockets in three X-ray crystal structures: HDM2·**13a** (PDB ID: 1YCR), HDM2·**7** (PDB ID: 2AXI), and HDM2·**3** (PDB ID: 2V2). The Trp and 6Cl-Trp shown in red are from the ligands (Trp in 1YCR, and Cl-Trp in 2AXI and 2V2). Only HDM2 residues within 5 Å of this (Cl)Trp are shown as stick representations. B) An alternative view shows the residues in HDM2 forming the Trp23 binding pocket together with their nearest distances [Å] from (Cl)Trp in the ligand. Note that the side chains of Phe86 and Leu57 adopt alternate conformations in the 2AXI structure.

ligand binding can occur, these two subdomains must move apart to expose the deep hydrophobic p53-binding pockets. In addition, the N-terminal segment of apo-HDM2 folds back, forming a lid over the shallow end of the p53-binding cleft, and this must also move away to allow access to the binding site.[17]

These data suggest a complex mechanism of binding of p53 to HDM2, which involves both displacement of water molecules from the surfaces of p53 and HDM2 and substantial conformational changes in both binding partners. In particular, the p53-binding pockets on HDM2 (once exposed) are quite hydrophobic in nature. The extent of their hydration prior to ligand docking is so far unknown, but would be expected to have a significant influence upon the thermodynamics of ligand binding.[18] In contrast, the cyclic β-hairpin p53 peptidomimetics appear by NMR spectroscopy to adopt relatively stable hairpin structures in free solution, so only relatively minor conformational changes appear necessary upon binding to HDM2.[10] Of course, these dynamic properties complicate a structure-based interpretation of thermodynamic binding data. However, one aim of this work was to characterize the *differences* in standard free energies of the three linear p53-derived peptides (**13**–**15**) and three cyclic β-hairpin peptidomimetics (**6**–**8**) in their binding to HDM2. Given the close similarities of the final ligand–protein structures, the data should then be informative with regard to the differences in binding between the linear and the cyclic peptides, and also for the interactions experienced by the 6-substituted tryptophans (6-Cl and 6-Me) within the Trp23 binding pocket.

Substituent effects upon ligand binding

Binding affinities were measured experimentally by two different methods: surface plasmon resonance (SPR) and isothermal titration calorimetry (ITC). Given that very similar, but nonidentical ligands were used for the two studies (Scheme 1), the close agreement observed between the affinities determined by these two different methods is reassuring (Tables 1 and 2).

We have shown here that the ligand side chain contributing most to binding between mimetic **7** and HDM2 is that of the 6-chloro-Trp3 residue (Table 3). We have also shown that the presence of the 6-Cl substituent on the indole ring of this ligand enhances the binding affinity—relative to the unsubstituted case—by a factor of 2–3, whereas the presence of a 6-Me substituent *weakens* the binding interaction by a factor of almost 2 (Table 1 and 2). This result was unexpected, because earlier studies with the linear peptides (**2**–**5**) showed that introduction of a 6-Cl, 6-Me, or 6-F substituent in the Trp side chain improved ligand affinity (IC_{50}) substantially, by factors of 63, 31, and 22, respectively.[6] Here we have also studied the affinities of p53-derived linear peptides (**13**–**15** and **16**–**18**) containing 6-Cl and 6-Me substituents in their Trp side chains towards HDM2. Now, through the introduction either of a 6-Cl or of a 6-Me group, affinity (K_D) improves by factors of up to 12 and 6, respectively (Table 1), results that are in much closer agreement to those obtained earlier with the analogues **2**–**5**. However, the question that then arises is why do the substituent effects on affinity differ so much in the linear and in the cyclic peptide ligands? The answer to this question is most likely linked to the quite different thermodynamic signatures that the linear and cyclic peptides show upon binding to HDM2.

Thermodynamic signatures

The standard free energies of binding of the linear (**13**–**15**) and the cyclic (**6**–**8**) peptides were measured by ITC. Although the binding of both is enthalpically driven (negative ΔH°), the enthalpic effects are three to four times (i.e., $\approx$10 kcal mol^{-1}) higher with the linear peptides at 298 K (Table 2; Figure 3A). This is presumably because the flexibilities of the linear peptide allow more favorable enthalpic interactions in the complexes than is possible for the more rigid cyclic peptides.

In addition, the binding of each cyclic peptide is characterized by a positive entropic $T\Delta S^\circ$ term, whereas those of the linear peptides show negative $T\Delta S^\circ$ values of similar magnitude. In other words, a constrained ligand experiences a re-

duced entropic penalty upon binding, as one might expect. One of the prime arguments frequently cited when designing conformationally constrained peptide ligands for protein receptors is that the constrained molecule should suffer a smaller entropic penalty, relative to the flexible linear peptide ligand, upon receptor binding, and this is certainly observed in this system. It is also clear, however, that the entropic penalty involved in binding the flexible linear peptide is largely offset in this system by an enhanced enthalpic gain upon interaction with HDM2.

When two hydrophobic molecules associate in aqueous solution, with consequent burial of hydrophobic surface, a *positive* standard entropy of binding ($T\Delta S^\circ$) would be expected, due to the release of ordered water molecules from the hydrophobic surfaces of protein and ligand into bulk water. Examples of *negative* values of both ΔH° and $T\Delta S^\circ$ in the association of molecules in water (with negative ΔG° values) are not exceptional, and have been known for a long time.[19] Although not consistent just with hydrophobic interactions, a negative standard entropy of binding could arise when, for example, attractive van der Waals interactions and hydrogen bonds are formed in the low-dielectric environment of the protein interface, and/or because of the requirement for folding of the linear p53-derived peptide into a regular α helix upon binding. It is again worth emphasizing, however, that the complex dynamic properties of the p53/HDM2 system complicate a structure-based interpretation of thermodynamic binding data.

Theoretical studies: interactions involving the substituents

Advances in computational methods promise greatly to facilitate the complex process of structure-based protein ligand design and the understanding of ligand–receptor interactions. Theoretical studies were therefore undertaken in an attempt to analyze the electronic natures of the interactions occurring between the various linear and cyclic peptides and HDM2 in a quantitative way; this information might in turn be helpful for deeper understanding of the substituent effects on the binding affinity and thermodynamic signatures discussed above.

The available X-ray crystal structures (vide supra) suggest (qualitatively, at least) that similar ligand–HDM2 interactions arise upon binding of both the linear and the cyclic peptides to HDM2. Upon closer analysis, however, some subtle structural differences become apparent. The crystal structure analysis of the HDM2·**7** complex, for example, identified alternate side chain conformations for HDM2 residues Phe86 and Leu57, which are buried deep within HDM2 and comprise part of the ligand X-Trp23 binding pocket. The energetically important X-Trp side chain of each ligand (where X = H, Cl, Me) binds close to both aliphatic (Leu57, Ile61, Val93, Ile99, and Ile103) and aromatic (Phe86 and Phe91) side chains in HDM2. In particular, the Phe86/Phe91 phenyl hydrogen atoms point towards the ligand-Trp indole 6-position (Figure 4). In the 2AXI structure it seems that the side chain of Phe86 can rotate, relative to its position in 1YCR and 2V2, most likely due to close interaction with the Cl substituent in the inhibitor **7**. A conformational grid search starting with the HDM2-**7** structure (PDB ID: 2AXI) was performed. The results of this analysis (not shown) suggest that even in the crystal there is sufficient flexibility in the binding site to allow the Phe86 and Phe91 side chains to adopt a wide range of χ_2 torsion angles.

Starting from the geometry given in the PDB structure 2AXI, the energies of interaction between the 6-substituents on the X-Trp ligands and the nearby Phe86/Phe91 residues were calculated. In the gas phase, the interaction energies are 2.4, 1.2, and 0.7 kcal mol^{-1} for X = Cl, X = Me, and X = H, respectively, whereas in a protein-like environment these interactions decrease to 1.5, 0.7, and 0.0, respectively (Table 4). The magnitudes of the interaction energies between these side chains and the X-Trp do depend upon the precise interaction geometries, and in particular upon the dielectric in the binding pocket (see the Supporting Information).

Overall, for 6-X-Trp in all ligands, the calculations suggest that small but significant stabilizing van der Waals interactions of the order of 0.7–1.5 kcal mol^{-1} can occur between either a polarizable Cl substituent or a Me substituent and the partial positive charge of the phenyl hydrogens of the Phe86/Phe91 side chains. However, with the methods available at present, the calculations are probably not sufficiently accurate to provide a reliable ranking of such individual small interaction energies, particularly given that the entire protein cannot be considered in this analysis. The calculations support the notion that introduction of the 6-Cl or 6-Me substituents into the energetically important Trp binding pocket should provide enhanced ligand affinity, due to the resulting van der Waals interactions with HDM2 residues Phe86 and Phe91, and provide a quantitative estimate for these interactions. This only partly accounts for the total effect on the affinity of the cyclic and linear peptides observed with the Trp substitutions. Other factors must also have an important role. For example, it can be observed in the crystal structure that there are also important van der Waals interactions arising from other residues in the binding site just above the plane of the indole ring (Figure 5), which also contribute to the overall stability of the ligand in the binding site. Depending on the substitution (X = Cl, CH_3, H) the resulting electronic nature of the π system will change, with corresponding strengthening or weakening of these van der Waals interactions.

Theoretical studies: hydrogen bonds

The indole NH groups of the 6-X-Trp residue in all three ligands (**3**, **7**, and **13a**) are close enough (2.7 Å for O···N in 2AXI) to hydrogen-bond to the backbone carbonyl group of Leu54 in HDM2 (Figure 1). We therefore used computational methods to estimate the strength of this ligand–protein H-bond and thus whether it is likely to contribute to the stabilization of the ligand·HDM2 complex. In the case of Cl substitution, the calculations predict that this interaction is worth 2.5 kcal mol^{-1} in a protein-like dielectric environment (Table 5), and would be even less in an environment with a dielectric similar to that of bulk water. Interestingly, theory also predicts that introduction of the 6-Cl substituent on the indole ring will strengthen the H-bond in the crystal structure geometry by $\approx$0.4 kcal mol^{-1},

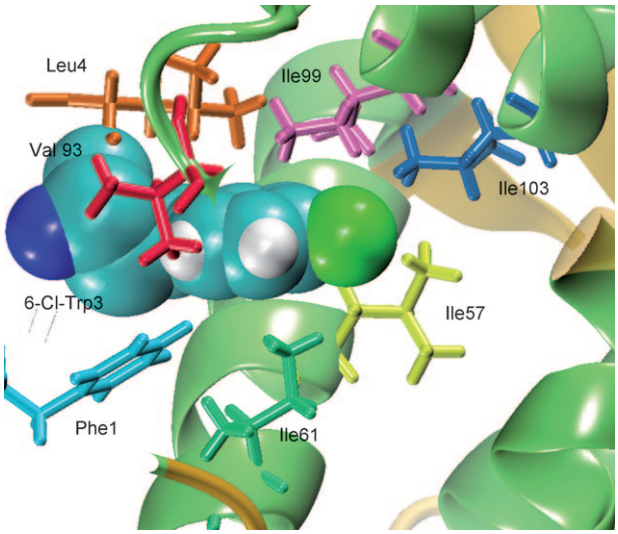

Figure 5. Interactions of Cl-Trp (in PDB 2AXI) with the nonaromatic side chains of HDM2 (Ile57: yellow, Ile61: green, Ile99: pink; Val93: red) and Leu4 (orange) of the ligand (compare with Figure 4).

relative to the ligand containing no substituent. A similar but smaller ($\approx$0.2 kcal mol^{-1}) strengthening effect is also seen when a 6-Me substituent is introduced.

These results provide a quantitative estimate of the stabilizing influence of one ligand–protein hydrogen bond in an environment with a protein-like interior dielectric. By extension it seems likely that the formation of multiple H-bonds along the backbone of the linear p53-derived peptide, as it folds into a helical conformation and binds to HDM2, may well have a significant impact on the thermodynamics of the overall binding reaction. The calculations furthermore highlight another way in which the 6-X substituent in the ligand can influence the stability of the ligand–HDM2 complex: namely through effects on H-bonding, in addition to the direct van der Waals interactions discussed above.

Theoretical studies: calculated binding energies

Currently, accurate prediction of ligand–receptor binding affinities by theoretical methods remains a major technical challenge. Nonetheless, the available structural and experimental binding data make these ligand–HDM2 interactions an interesting model system to examine with state-of-the-art theoretical methods. The approach we have used here to calculate binding energies, and in particular, binding energy differences between the various ligands of HDM2, involves solving the linearized Poisson–Boltzmann equation to determine electrostatic interaction energies. The calculated total binding energy differences ($\Delta E_{\text{tot binding}}$) provided by the adaptive Poisson–Boltzmann solver (APBS) method[11] includes electrostatic interactions ($\Delta E_{\text{tot elect}}$) arising from both Coulombic (ΔE) and polar solvation ($\Delta E_{\text{solvation}}$) contributions, as well as nonpolar solvation effects ($\Delta E_{\text{tot nonelect}}$) arising from cavitation and dispersion terms. The calculations, however, do not fully account for the changes in entropy that occur upon binding, and so the calculated binding energy differences ($\Delta E_{\text{tot binding}}$) are not quantitatively comparable to the experimentally determined standard free energy of binding (ΔG°), nor to experimentally determined ΔH° and $T\Delta S^\circ$ values. The values both of $\Delta E_{\text{tot binding}}$ and of $\Delta\Delta H^\circ$ will certainly be influenced by changes in the electrostatic properties of the bound ligand as the structure is varied (for example, linear vs. cyclic ligand, chloro vs. methyl substituent, etc.), and so correlations between *binding energy differences* predicted by theory and those observed experimentally might be expected, and are indeed found, as discussed below.

With this in mind, a comparison was made of the experimentally determined thermodynamic parameters (Table 2) and the calculated electrostatic interaction energy differences. The results of the comparison are summarized in Figure 3, and show interesting correlations between experimental and theoretical data. For example, a stronger total binding energy ($\Delta E_{\text{tot binding}}$) is calculated for the linear peptide **13a** than for its cyclic counterpart **7** (Figure 3B, red bars), which correlates with the larger ΔH° values determined for the linear peptides than for the cyclic peptides by ITC (Figure 3A, orange bars). Interestingly, this is shown to arise computationally from a difference in the nonpolar contributions to solvation ($\Delta E_{\text{tot nonelect}}$) in the two systems (green bars), since the direct ligand–receptor total electrostatic interactions ($\Delta E_{\text{tot elect}}$) are not greatly different (Figure 3B, orange bars). Thus, $\Delta E_{\text{tot elect}} = \Delta E_{\text{elect}} + \Delta E_{\text{solvation}}$ (see above), and so ΔE_{elect} (Figure 3B, yellow hatched) is more favorable in the linear molecules than in the cyclic ones, $\Delta E_{\text{solvation}}$ (Figure 3B, blue hatched) is more unfavorable in the linear molecules than in the cyclic systems, with the net result (stated above) that the $\Delta E_{\text{tot elect}}$ values (orange bars) are not hugely different for these two systems (Table 6).

When we consider the changes in the calculated total binding energy ($\Delta E_{\text{tot binding}}$) caused by varying the substituent in the 6-X-Trp residue (relative to the case in which X = H), a small increase is found for both substituents (Cl and Me; Figure 3C, red bars). However, the advantage of having X = Cl over X = Me is predicted by calculation to be more pronounced in the cyclic ligands than in the linear ligands. The gain in calculated total binding energy is thus much smaller for X = Me in the cyclic case, whereas the introduction of Cl and Me gives a significant gain for the linear ligand. Indeed, for X = Me the $\Delta E_{\text{tot elect}}$ component is unfavorable for both the linear and cyclic peptides, but much more so in the cyclic case than for the linear peptide (Figure 3C, orange bars). For this

Table 6. Computational results for energetic contributions to the binding energies between the HDM2 receptor and p53 peptidomimetics 2AXI-(**6**–**8**) and 1YCR-(**13**–**15**). Results are expressed relative to tryptophan (X = H) in terms of energy difference ($\Delta\Delta$).

Complex	$\Delta\Delta E_{\text{tot elect}}$ [a]	$\Delta\Delta E_{\text{tot nonelect}}$ [b]	$\Delta\Delta E_{\text{tot bind}}$ [c]	$\Delta\Delta E_{\text{expt}}$ [d]
2AXI-**7** (X = Cl)	−0.95	−4.14	−5.09	−0.65
2AXI-**8** (X = Me)	1.83	−3.12	−1.30	0.17
1YCR-**14** (X = Cl)	−1.51	−1.90	−3.42	−0.72
1YCR-**15** (X = Me)	0.34	−3.03	−2.69	−0.66

[a] Total electrostatic contribution; [b] total nonelectrostatic contribution; [c] total binding energy; [d] experimentally determined binding energy.

reason, $\Delta E_{\text{tot binding}}$ is also much smaller for the cyclic ligand with introduction of X=Me. Experimentally, we observe that addition either of a Me or of a Cl substituent in the linear peptides increases affinity, whereas addition of Cl in the cyclic ligand improves affinity but addition of Me slightly weakens it (Table 2). Interestingly, this experimentally observed weakening of affinity upon addition of Me in the cyclic ligand (but not the linear ligand) is reflected in the results of the calculations shown in Figure 3C.

This trend can also be illustrated with a surface electrostatic representation. Thus, in Figure 6 the calculated *differences* in molecular electrostatic potentials (MEPs) are shown for the

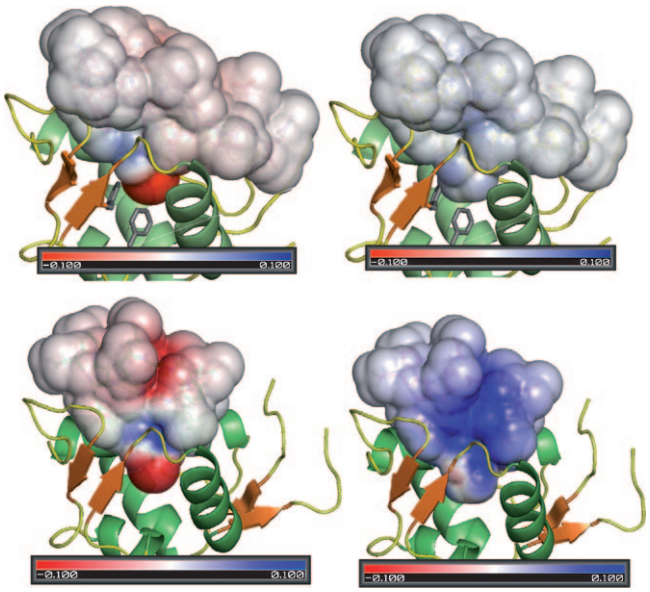

Figure 6. HDM2–ligand complexes. The top set represents the molecular electrostatic potential map difference between X=Cl and X=H (left-hand side) and between X=Me and X=H (right-hand side) in the bound linear peptide (as in 1YCR). The lower set display the molecular electrostatic potential map difference between X=Cl and X=H (left-hand side) and between X=Me and X=H (right-hand side) in the bound cyclic peptide (as in 2AXI).

complexes with linear (top) and cyclic (bottom) ligands, for the case of X=Me relative to X=H (left-hand side), and for the case of X=Cl relative to X=H (right-hand side). The largest effects are observed in complexes with the cyclic peptides, in which additional positive charge is indicated by blue and additional negative charge is indicated by red. We emphasize that the calculations are not sufficiently accurate to provide reliable quantitative estimates of such small energetic effects, but the calculations highlight what types of subtle differences in electrostatic properties of the ligands may result upon addition either of Cl or of Me as a substituent in the Trp residue.

The ability of this theoretical approach to reflect experimentally determined thermodynamic features of the binding reactions correctly for this series of peptide ligands and to provide insights into the electronic natures of the interactions is notable. Such peptide–protein interactions remain interesting targets for the further development of the peptidomimetic approach to protein–ligand design, as well as of computational methods for the analysis of protein–ligand interactions, especially for the difficult case of discovering protein–protein interaction inhibitors.

Acknowledgement

We thank the Swiss National Science Foundation for supporting this work.

Keywords: calorimetry · computational chemistry · protein–protein interactions · surface plasmon resonance

[1] J. K. Murray, S. H. Gellman, *Biopolymers* **2007**, *88*, 657.
[2] A. Shmueli, M. Oren, *Mol. Cell* **2007**, *25*, 794.
[3] P. Chène, *Mol. Cancer Res.* **2004**, *2*, 20.
[4] L. T. Vassilev, *J. Med. Chem.* **2005**, *48*, 4491.
[5] P. H. Kussie, S. Gorina, V. Marechal, B. Elenbaas, J. Moreau, A. J. Levine, N. P. Pavletich, *Science* **1996**, *274*, 948.
[6] C. García-Echeverría, P. Chène, M. J. J. Blommers, P. Furet, *J. Med. Chem.* **2000**, *43*, 3205.
[7] K. Sakurai, C. Schubert, D. Kahne, *J. Am. Chem. Soc.* **2006**, *128*, 11000.
[8] B. L. Grasberger, T. Lu, C. Schubert, D. J. Parks, T. E. Carver, H. K. Koblish, M. D. Cummings, L. V. LaFrance, K. L. Milkiewicz, R. R. Calvo, D. Maguire, J. Lattanze, C. F. Franks, S. Zhao, K. Ramachandren, G. R. Bylebyl, M. Zhang, C. L. Manthey, E. C. Petrella, M. W. Pantoliano, I. C. Deckman, J. C. Spurlino, A. C. Maroney, B. E. Tomczuk, C. J. Molloy, R. F. Bone, *J. Med. Chem.* **2005**, *48*, 909.
[9] R. Fasan, R. L. A. Dias, K. Moehle, O. Zerbe, D. Obrecht, P. R. E. Mittl, M. G. Grutter, J. A. Robinson, *ChemBioChem* **2006**, *7*, 515.
[10] R. Fasan, R. L. A. Dias, K. Moehle, O. Zerbe, J. W. Vrijbloed, D. Obrecht, J. A. Robinson, *Angew. Chem.* **2004**, *116*, 2161; *Angew. Chem. Int. Ed.* **2004**, *43*, 2109.
[11] N. A. Baker, D. Sept, S. Joseph, M. J. Holst, J. A. McCammon, *Proc. Natl. Acad. Sci. USA* **2001**, *98*, 10037.
[12] R. Dawson, L. Müller, A. Dehner, C. Klein, H. Kessler, J. Buchner, *J. Mol. Biol.* **2003**, *332*, 1131.
[13] S. Bell, C. Klein, L. Müller, S. Hansen, J. Buchner, *J. Mol. Biol.* **2002**, *322*, 917.
[14] H. Lee, K. H. Mok, R. Muhandiram, K.-H. Park, J.-E. Suk, D.-H. Kim, J. Chang, Y. C. Sung, K. Y. Choi, K.-H. Han, *J. Biol. Chem.* **2000**, *275*, 29426.
[15] O. Schon, A. Friedler, S. Freund, A. R. Fersht, *J. Mol. Biol.* **2004**, *336*, 197.
[16] S. Uhrinova, D. Uhrin, H. Powers, K. Watt, D. Zheleva, P. Fischer, C. McInnes, P. N. Barlow, *J. Mol. Biol.* **2005**, *350*, 587.
[17] S. A. Showalter, L. Bruschweiler-Li, E. Johnson, F. Zhang, R. Brüschweiler, *J. Am. Chem. Soc.* **2008**, *130*, 6472.
[18] S. W. Homans, *Drug Discovery Today* **2007**, *12*, 534.
[19] P. D. Ross, S. Subramanian, *Biochemistry* **1981**, *20*, 3096.

Received: January 5, 2009
Published online on April 30, 2009

